Microfluidic transport through micro-sized holes treated by non-equilibrium atmospheric-pressure plasma

Takumi Ito[1], Kenji Ishikawa[1], Daisuke Onoshima[1], Naoto Kihara[2], Kentaro Tatsukoshi[2], Hidefumi Odaka[2], Hiroshi Hashizume[1], Hiromasa Tanaka[1], Hiroshi Yukawa[1], Keigo Takeda[1], Hiroki Kondo[1], Makoto Sekine[1], Yoshinobu Baba[1], and Masaru Hori[1]

[1] *Nagoya University, Furo-cho, Chikusa-ku, Nagoya, Aichi 464-8603 Japan*

[2] *Asahi Glass Co., Ltd., 1-5-1, Marunouchi, Chiyoda-ku, Tokyo 100-8405 Japan*

Corresponding address: ishikawa.kenji@nagoya-u.jp

Abstract

In the field of microfluidics, it is possible to facilitate liquid transport through micro-sized holes with large slip lengths by lowering the friction at the interface between the flow and the inner surface of the holes. In this paper, we discuss the use of non-equilibrium atmospheric-pressure plasma to modify the surface wettability of micro-sized holes in glass substrates that are similar to those used as flow channels in glass microfiltration devices. In our experiments, liquid transport flows were driven by internal Laplace pressure differences based on the surface tensions of droplets placed on the front and back sides of the tested substrates.

I. INTRODUCTION

In recent years, microfluidic devices have received significant attention in a number of technological fields, including those involving single cell trapping and analysis [1-4]. Using newly developed techniques, it has now become possible to deal with metabolomics [5] and cancer biology [6] at the single cell level. Indeed, one of the most significant new developments achieved in the field of cancer biology utilizes single cell trapping technology to detect very low concentrations of circulating tumor cells (CTCs) buried in the background of millions of normal hematopoietic cells [7-10]. This technology facilitates improved trapping of single cells on biochips so that they can be applied to one of several analysis techniques [11].

In microfluidic devices, cell-trapping motions are typically controlled by the application of electric fields, magnetic fields, or centrifugal force [12-14]. However, since these may stimulate or impose environmental stress on the captured cells [5], an alternative, minimally invasive cell trapping method is needed.

Since the diameters of the targeted cells ranges from 10 to 30 microns, using substrates equipped with holes that are smaller than the target cells can provide a function that allows single cells to be trapped individually. While technologies based on single cell filtration have previously been suggested, it has also been pointed out that

exacting microfluidic control would be essential to the development of a minimally invasive cell capture method [11, 15-17]. One simple microfluidic device mechanism utilizes a suspension fluid to transport the cells and traps single cells on substrates equipped with micro-sized holes [18, 19]. More specifically, the cell trapping function is provided by a liquid transport traveling through the micro-sized holes combined with a microfluidic control for dispersing the cells [20]. Thus, the behavior of liquid transport through the micro-sized holes is of particular importance [15].

At the micro- and nano-length scales, the flow of liquids such as water and blood depends on the length scale of the flow. Assuming a Poiseuille-type flow, defined as an incompressible Newtonian fluid in a laminar flow through a long *x*-direction cylindrical tube, the flow velocity v_x at the centerline of an infinite cylindrical tube yields:

$$v_x = \frac{h^2}{4\mu}\left(-\frac{\mathrm{d}p}{\mathrm{d}x}\right)\left[1-\left(\frac{y}{h}\right)^2+\frac{2\beta}{h}\right], \quad (1)$$

where h is the radius of the cylindrical tube, μ is the viscosity, $\left(-\frac{\mathrm{d}p}{\mathrm{d}x}\right)$ is the pressure drop, and β is the extrapolation or slip length [21]. The first term in the $1-\left(\frac{y}{h}\right)^2$ bracket is the standard solution for the pressure-driven Stokes flow, where the flow velocities are very slow in a cylindrical tube with no slip, while the second term, $\frac{2\beta}{h}$ represents an additional velocity associated with the boundary condition, in this case, the fluid friction resistance [22]. As h decreases, the second term can become significant

and dominate at the micro-scale. Hydrophobic surfaces have frequently been reported as exhibiting large slip lengths, i.e. low flow resistance [23-26]. Conversely, there are a few reports stating that hydrophilic surfaces provide low flow resistance, because water droplets are known to spread rapidly on super-hydrophilic flat surfaces [27]. In one such report, Joseph and Tabeling showed that the use of a smooth hydrophilic surface resulted in both large flow velocities and slip lengths in a 10 μm × 100 μm microchannel [28]. However, to the best of our knowledge, no consensus has yet been reached on the relationship between hydrodynamic resistance and wettability.

It has previously been reported that surface wettability is particularly affected by the cleanliness of the flat surface glass substrates, for example, due to the absence or presence of organic contaminants [29-32]. With this point in mind, we also note that the use of non-equilibrium atmospheric pressure plasma (NEAPP) to clean such substrates provides numerous advantages. For example, several types of materials are compatible with NEAPP cleaning owing to the low temperature, high throughput, and large processing area of the method [33-36]. Additionally, the absence of a vacuum system helps to reduce equipment costs. The NEAPP process also has the potential for application to the specific structure of a local surface, such as the interior of high-aspect-ratio, micro-sized holes, in order to control wettability.

In this paper, we demonstrate the utilization of wettability control by means of NEAPP treatments applied to the interiors of high-aspect-ratio, micro-sized holes in order to stabilize liquid transport through them. We also report on the development of a method for evaluating the plasma treatment of hole interiors and our analysis of liquid transport rates through these holes. The use of NEAPP treatments has made it possible to achieve fast liquid transports that are driven by droplet internal pressure differences.

II. EXPERIMENTAL

A. Materials

We used alkali-free glass substrates with thicknesses of 150 or 200 μm (AN-100, Asahi Glass Co., Ltd.). Open micro-sized, high-aspect-ratio holes were fabricated by the thermal etching method using a femtosecond ultraviolet (UV) laser. Figure 1 shows (a) top-view and (b) bottom-view images of the sample taken by an optical microscope, as well as a (c) cross-sectional image taken by a scanning electron microscope (SEM). Two sample types were prepared. One sample type containing a 40 × 40 array of holes was fabricated with a pitch of 50 μm on 150-μm-thick substrates. The top holes were approximately 14 μm in size while the bottom holes were approximately 4 μm. The other sample type contained a 10 × 10 array of holes with a pitch of 200 μm on 200-μm-thick substrates. In this sample type, the sizes for the top holes ranged from 13

to 23 μm, while those of the bottom holes ranged from 3 to 6 μm. After fabrication, the samples were cleaned and stored under ambient atmospheric conditions without clean air circulation.

B. Nonequilibrium atmospheric pressure plasma treatments

Figure 1(d) shows a schematic diagram of the NEAPP equipment used in our study [33]. The plasma is excited by a high-voltage alternating current (AC) power supply that provides a half peak voltage of 7 $kV_{0\text{-}P}$ for a sinusoidal waveform with a frequency of 60 Hz. Argon (Ar) gas was supplied at a flow rate of 3 standard liters per minute (SLM). For cooling, nitrogen (N_2) gas was supplied to the two electrodes of the apparatus at a flow rate of 5 SLM. The plasma characteristics were as follows: plasma density, ~2×10^{16} cm^{-3}; O atom density, ~5×10^{14} cm^{-3}; and gas temperature, ~1800 K. These characteristics were analyzed by vacuum ultraviolet absorption (VUVAS) and optical emission spectroscopy, as previously reported [33].

The glass substrate was set on an experimental stage with a gap of approximately 11 mm from the surface of the stage to the substrate bottom. The top of the glass surface was separated from the plasma head by a distance of 10 mm. Under these conditions, a plasma flare consisting of a curtain of excited plasma approximately 20 mm wide and 10 mm long, was emitted from the head. Thus, the end of the plasma flare was in direct

contact with the hole regions fabricated on the glass surface. Note that the hole morphologies were not changed by the treatment because no etching of glass had taken place. The changes in wettability were primarily due to chemical oxidation reactions [31].

C. Evaluation of liquid transport

Contact angle measurements of water droplets on the tested glass substrates were then carried out using a computerized contact angle measuring system (DSA100, Krüss GmbH, Germany). Figure 2(a) shows a typical image of a measurement taken after dropping approximately 1 μl of water on the horizontal plane of a glass surface. When the volume of liquid is very small, it can be assumed that the resulting droplet will be shaped like a segment of a sphere and that the droplet volume, *V*, can be expressed by [37]

$$V = \pi r_{\mathrm{d}}^3 \left(\frac{2}{3} - \cos\theta + \frac{1}{3}\cos^3\theta\right),$$

where r_{d} is the droplet radius and θ is the contact angle, as is schematically shown in Fig. 2(b). According to the Laplace equation given by [38], a spherical droplet of radius r_{d} and surface tension γ is surrounded by the external medium with a pressure P_l,

$$P_l = 2\gamma / r_{\mathrm{d}} \quad . \qquad (2)$$

Under atmospheric pressure P_{a}, the internal pressure of droplet P_{d} is expressed by

$P_d = P_a + 2\gamma/r_d$. As the droplet radius decreases, the internal pressure of the droplet increases [39].

Figure 2(c) schematically depicts the liquid transport that results from a difference in pressure $P_t - P_b$ between two droplets, where P_t is the pressure of the top droplet and P_b is the pressure of the bottom droplet. Liquid transport through the holes is enhanced as the internal pressure of the droplet on the front surface becomes larger than the internal pressure of droplet on the back surface.

Prior to the liquid transport stage, an approximately 2 μl water droplet is applied to the back surface of the substrate, where it spreads to cover the entire target area of the hydrophilic glass surface. Capillary action causes the liquid to penetrate into all of the open micro-sized holes. Next, the glass substrate is carefully turned around and a water droplet with a volume of approximately 1 μl is applied to the front surface of the substrate. Because the internal pressure of the front surface droplet is larger than that of the back surface droplet, the pressure difference causes water to flow from the front side to the back side of the substrate through the holes. Internal pressure of the water droplet is hydrostatically applied with uniform capillary-action among them whole.

Liquid transportation rates were then evaluated based on temporal reductions in the droplet volumes on the front surface, which were estimated by Eq. 2 using parameters r_d

and θ. The temporal behavior was fitted to a quadratic function, $V = \mathrm{A}t^2 + Bt + V_0$, where V_0 is an initial volume and A and B are parameters. The initial rate of droplet volume reduction was given by the coefficient B.

III. RESULTS AND DISCUSSION

Figure 3(a) shows the temporal changes to the water volume on the front surface of the sample after the droplet was applied. In the case of a flat glass surface without holes, the droplet volume decreased gradually as time elapsed at the measured volume reduction rate of approximately 1.3 nl/s. This corresponded well with the estimated value (approximately 1.5 nl/s) of the evaporation rate of water from based on the contact length lc of a droplet on a flat glass surface (Fig. 2(b)) [37]. We note that the identical plasma irradiation for 10 s at minimum provides super-hydrophilic surfaces, when a flat glass substrate without holes.

In the case of using an unclean (before plasma treatment) glass substrate with holes, the volume reduction rate was approximately 1.3 nl/s (Fig. 3(b)). This means that the reduction in droplet volume was due to evaporation alone. Therefore, when an unclean substrate was used, super-hydrophilicity was not present (contact angle of approximately 40°) and the liquid did not transport through the holes, possibly due to contamination occurring on the inner surface of the open holes just after fabrication.

Regardless of the hole density of both 10×10 and 40×40, the initial hydrophobic surface prevented to transport through the holes from front to back.

Next, the effects of plasma treatment on the interior of holes for substrate samples back surfaces which had been treated by one-sided plasma irradiation for 10, 60, and 180 s were examined. Figure 3(b) shows the reduction rates resulting from different plasma irradiation durations. In samples irradiated with a NEAPP of Ar for 10 s, a rate of 2.1 nl/s was observed, while a rate of 3.0 nl/s was observed for 60 s, and 5.2 nl/s was observed for 180 s. As the plasma irradiation durations increased, the rates of reduction in the water volume increased, as shown in Fig. 3(a). This indicates that plasma treatment enhanced the liquid transport through the holes from the front side of the sample to its back side.

Table 1 lists the contact angles and pressure differences between droplets on the front surface and back surfaces of the samples. The back surface contact angle before plasma treatment was approximately 40º. The slight variations in the contact angles among the samples were believed to be caused by surface contaminants. After plasma treatment for 10 s, the contact angle of the back surface decreased to approximately 2º, thereby indicating the presence of super-hydrophilicity. The contact angles were almost same when the plasma irradiation time was increased to 60 and 180 s. Estimated pressure

differences between droplets on the front and back surfaces were calculated using Eq. 2. Before the plasma treatment, the pressure difference was 1.6 kPa. For the sample treated by plasma irradiation for 10 s, the pressure difference became more than four times larger, 6.9 kPa. Those pressure differences remained relatively constant as the plasma irradiation time increased from 10 to 180 s, thereby indicating that 10 s is sufficient for the substrate surface treatment.

As listed in Table 1, although the wettability and the pressure differences were almost the same, plasma irradiation for durations of more than 10 s led to faster liquid transport rates. This could be interpreted as indicating that the liquid transport enhancement was the result of higher hydrophilicity surface states within the hole. It has been previously noted that the surface state affects the velocity of the fluid-solid interface [40, 41]. In our study, we are particularly interested in the phenomenon whereby super-hydrophilicity enhances liquid transport through micron-sized holes.

When the hole diameters were changed, the liquid transport rates were found to be different as well. Figure 4 shows that when different diameter holes were fabricated and examined on 10 × 10 hole 200-μm-thick (red filled circles) substrates irradiated with plasma for 180 s, the larger hole diameters resulted in faster liquid transport rates. Given that the estimated pressure differences were approximately 10 kPa, this agrees with the

Hagen-Poiseuille law, which states that flow velocities are proportional to the fourth power of a tube radius [21]. The data were well fitted by the quartic function of diameters as indicated a solid line in Fig. 4.

We observed that faster liquid transport could be achieved by hydrophilic treatment of NEAPP (Fig. 3(a)). In their experiments, Tretheway and Meinhart reported a measured slip length of approximately 1 μm on hydrophobic surfaces, and slip lengths of zero on hydrophilic surfaces [22]. Voronov *et al.* argued that, based on molecular dynamics simulations, higher hydrophobicity alone did not change the slip lengths. However, when higher hydrophobicity was combined with smoother surfaces, larger slip lengths would appear [42]. In contrast, our results indicate that super-hydrophilic surfaces provide larger liquid transport rates due to lower friction and larger slip lengths. In the literatures, Sakai *et al* showed a highly hydrophilic TiO_2 surface reduced the fluid friction [43]. This report supports our experimental results where, in actual micro-scaled situations, surface wettability was found to contribute significantly to liquid transport flow rates. For flow enhancement, the NEAPP treatments of the hole interior were found to effectively enhance the flow transport caused by pressure differences generated by internal Laplace droplet pressures.

Finally, considering the flow integration through each hole, the water pressure

gradient, and the inverse proportionality to the hole depth, the observed liquid transport should also be proportional to the number of holes and inversely proportional to the substrate thickness. When the three parameters consisting of the number of holes (1600 over 100), the glass substrate thickness (150 over 200 μm), and pressure gradient (7 over 10 kPa) were normalized, the liquid transport rate was estimated to be as normalized line as indicated with dashed line in Fig. 4. The liquid transport rates coincides with theoretical values after the four parameters (number of holes, averaged hole diameters, hole lengths, and pressure gradient) were normalized. Nevertheless, it is indisputable that the flow velocity distribution inside the holes may be affected by inner surface wettability, since the interior morphology of each sample may be different. Thus, the interior of the holes may have an impact on the flow velocity. Unfortunately, we have not yet been able to reach a satisfactory solution for this problem and further investigations will be required to resolve the issue.

IV. CONCLUSION

We demonstrated that the application of non-equilibrium atmospheric pressure (NEAPP) processes to the interiors of high-aspect-ratio, micro-sized holes facilitated the stability of liquid transportation through those holes. After plasma treatment, liquid transport rates through the holes from the front to back sides of the experimental

substrates were significantly enhanced due modifications to the back surface contact angle from 40º to 4º due to the presence of super-hydrophilicity. The droplet pressure difference between the front and back surfaces increased more than 4-fold, 6.9 kPa. As the plasma irradiation durations increased, liquid transport rates through the holes from the front to the back side of the substrate became faster. This is believed to be the result of plasma irradiation modifications to hole interior surfaces that allow more slippage in slip boundary conditions, thus enhancing liquid transport. The results of our experiments show that the use of NEAPP processes can modify the chemical states of substrate surfaces, thereby enhancing liquid transport through the interiors of micro-sized holes.

Acknowledgments

This research is partially supported by the Center of Innovation Program (Nagoya-COI) of the Japan Science and Technology Agency (JST).

References

[1] N. Kaji, and Y. Baba, "Nanobiodevice-based Single Biomolecule Analysis, Single-Cell Analysis," Anal. Sci., vol. 30, pp. 859-864, 2014.

[2] S. Byun, S. Son, D. Amodei, N. Cermak, J. Shaw, J. H. Kang, V. C. Hecht, M. M. Winslow, T. Jacks, P. Mallick, and S. R. Manalis, "Characterizing deformability and surface friction of cancer cells," Proc. Natl. Acad. Sci. USA., vol. 110, no. 19, pp. 7580-7585, 2013.

[3] N.-T. Huang, W. Chen, B.-R. Oh, T. T. Cornell, T. P. Shanley, J. Fu, and K. Kurabayashi, "An integrated microfluidic platform for *in situ* cellular cytokine secretion immunophenotyping," Lab Chip, vol. 12, pp. 4093-4101, 2012.

[4] T. M**ü**ller, D.A. White, and T. P. J. Knowles, "Dry-mass sensing for microfluidics," Appl. Phys. Lett., vol. 105, pp. 214101(1-4), 2014.

[5] R. Zenobi, "Single-Cell Metabolomics," Science, vol. 342, pp. 1243259(1-10), 2013.

[6] P. Li, Z. S. Stratton, M. Dao, J. Ritz, and T. J. Huang, "Probing circulating tumor cells in microfluidics," Lab Chip, vol. 13, pp. 602-609, 2013.

[7] S. Zheng, H. K. Lin, B. Lu, A. Williams, R. Datar, R. J. Cote, and Y.-C. Tai, "3D microfilter device for viable circulating tumor cell (CTC) enrichment from blood, Biomed," Biomed. Microdevices, vol. 13, no. 203, pp. 203-213, 2011.

[8] K. Hoshino, Y.-Y. Huang, N. Lane, M. Huebschman, J. W. Uhr, E. P. Frenkel, and X. Zhang, "Microchip-based immunomagnetic detection of circulating tumor cells," Lab Chip, vol. 11, pp. 3449-3457, 2011.

[9] S. Nagrath, L. V. Sequist, S. Maheswaran, D. W. Bell, D. Irimia, L. Ulkus, M. R. Smith, E. L. Kwak, S. Digumarthy, A. Muzikansky, P. Ryan, U. J. Balis, R. G.

Tompkins, D. A. Haber, and M. Toner, “Isolation of rare circulating tumour cells in cancer patients by microchip technology,” Nature, vol. 450, pp. 1235-1239, 2007 .

[10] P. G. Schiro, M. Zhao, J. S. Kuo, K. M. Koehler, D. E. Sabath, and D. T. Chiu, “Sensitive and High-Throughput Isolation of Tare Cells from Peripheral Blood with Ensemble-Decision Aliquot Tanking,” Angew. Chem. Int. Ed., vol. 51, pp. 4618-4622, 2012.

[11] A. L. Hook, D. G. Anderson, R. Langer, P. Williams, M. C. Davies, and M. R. Alexander, “High throughput methods applied in biomaterial development and discovery,” Biomater., vol. 31, pp. 187-198, 2010.

[12] T. Obata, “The Development of Medical Devices Using MEMS Technology,” Hyomen-Gijutsu (in Japanese), vol. 59, no. 6, pp. 382-386, 2008.

[13] D. M. C. RoyChaudhuri, L. Das, and J. Chatterjee, “Microtrap electrode devices for single cell trapping and impedance measurement,” Biomed. Microdevices, vol. 14, pp. 955-964, 2012.

[14] S.-W. Lee, J. Y. Kang, I.-H. Lee, S.-S. Ryu, S.-M. Kwak, K.-S. Shin, C. Kim, H.-I. Jung, and T.-S. Kim, “Single-cell assay on CD-like chip using centrifugal massive single-cell trap,” Sensor. Actuator A, vol. 143, pp. 64-69, 2008.

[15] F. A. W. Coumans, G. V. Dalum, M. Beck, and L. W. M. M. Terstappen, “Filtration Parameters Influencing Circulating Tumor Cell Enrichment from Whole Blood,” PLoS One, vol. 8, no. 4, pp. e61774, 2013.

[16] D. J. Collins, T. Alan, and A. Neild, “The particle valve: On-demand particle trapping, filtering, and release from a microfabricated polydimethylsiloxane

membrane using surface acoustic waves," Appl. Phys. Lett., vol. 105, pp. 033509(1-4), 2014.

[17] R. Dey, S. DasGupta, and S. Chakraborty, "Thermally activated control of microfluidic friction," Appl. Phys. Lett., vol. 101, pp. 134101(1-5), 2012.

[18] A. Y. Lau, P. J. Hang, A. R. Wu, and L. P. Lee, "Open-access microfluidic patch-clamp array with raised lateral cell trapping sites," Lab Chip, vol. 6, pp. 1510-1515, 2006.

[19] M. Hosokawa, M. Asami, S. Nakamura, T. Yoshino, N. Tsujimura, M. Takahashi, S. Nakasono, T. Tanaka, and T. Matsunaga, "Leukocyte Counting From a Small Amount of Whole Blood Using a Size-Controlled Microcavity Array," Biotechnol. Bioeng. vol. 109, no. 8, pp. 2017-2024, 2012.

[20] D. L. Adams, P. Zhu, O. V. Makarova, S. S. Martin, M. Charpentier, S. Chumsri, S. Li, P. Amstutz, and C.-M. Tang, "The systematic study of circulating tumor cell isolation using lithographic microfliters," RSC Adv., vol. 4, pp. 4334-4342, 2014.

[21] J. H. Spurk, "Fluid Mechanics", (Springer-Verlag Berlin Heidelberg, 2008).

[22] D. C. Tretheway and C. D. Meinhart, "Apparent fluid slip at hydrophobic microchannel walls," Phys. Fluids, vol. 14, no. 3, pp. L9-L12, 2002.

[23] A. V. Belyaev, and O. I. Vinogradova, "Hydodynamic interaction with

super-hydrophobic surfaces," Soft Matter, vol. 6, pp. 4563-4570, 2010.

[24] B. A. Maali and B. Bhushan, "Measurement of slip length on superhydrophobic surfaces," Phil. Trans. Royal. Soc. A, vol. 370, pp. 2304-2320, 2011.

[25] D. C. Tretheway and C. D. Meinhart, "A generating mechanism for apparent fluid slip in hydrophobic microchannels," Phys. Fluids., vol. 16, no. 5, pp. 1509-1515, 2004.

[26] R. S. Voronov, D. V. Papavassiliou, and L. L. Lee, "Slip length and contact angle over hydrophobic surfaces," Chem. Phys. Lett., vol. 441, pp.273-276, 2007.

[27] K.-H. Chu, R. Xiao, and E. N. Wang, "Uni-directional liquid spreading on asymmetric nanostructured surfaces," Nat. Mater. vol. **9**, pp. 413-417, 2010.

[28] P. Joseph and P. Tabeling, "Direct measurement of the apparent slip length," Phys. Rev. E, vol. 71, pp. 035303(1-4), 2005.

[29] M. Iwasaki, Y. Matsudaira, K. Takeda, M. Ito, E. Miyamoto, T. Yara, T. Uehara, and M. Hori, "Roles of oxidizing species in a nonequilibrium atmospheric pressure pulsed remote O_2/N_2 plasma glass cleaning process," J. Appl. Phys., vol. 103, pp. 023303(1-7), 2008.

[30] M. Iwasaki, K. Takeda, M. Ito, T. Yara, T. Uehara, and M. Hori, "Effect of low level O_2 addition to N_2 on surface cleaning by nonequilibrium atmospheric pressure

pulsed remote plasma," J. J. Appl. Phys., vol. 46, no. 23, pp. L540-542, 2007.

[31] M.C. Kim, D. K. Song, H.S. Shin, S.-H. Baeg, G.S.Kim, J.-H. Boo, J. G. Han, and S. H. Yang, "Surface modification for hydrophilic property of stainless steel treated by atmospheric-pressure plasma jet," Surf. Coat. Technol., vol. 171, pp. 312-316, 2003.

[32] J.-S. Kwon, Y. H. Kim, E. H. Choi, and K.-N. Kim, "Development of ultra-hydrophilic and non-cytotoxic dental vinyl polysiloxane impression materials using a non-thermal atmospheric-pressure plasma jet," J. Phys. D: Appl. Phys., vol. 46**,** pp. 195201(1-5), 2013.

[33] M. Iwasaki, H. Inui, Y. Matsudaira, H. Kano, N. Yoshida, M. Ito, and M. Hori, "Nonequilibrium atmospheric pressure plasma with ultrahigh electron density and high performance for glass surface cleaning," Appl. Phys. Lett., vol. 92, pp. 081503(1-3), 2008.

[34] O. Sakai, Y. Kishimoto, and K. Tachibana, "Integrated coaxial-hollow micro dielectric barrier discharges for a large area plasma source operating at around atmospheric pressure," J. Phys. D: Appl. Phys. Vol. 38, pp. 431-441, 2005.

[35] D. Wang, D. Zhao, K. Feng, X. Zhang, D. Liu, and S. Yang, "The cold and atmospheric-pressure air surface barrier discharge plasma for large area sterilization

applications,” Appl. Phys. Lett., vol. 98, pp. 161501(1-2), 2011.

[36] S. Wang, J. Wan, X. Jia, and L. Zhao, “Surface Treatment of Flat Panel Display Substrates by a Uniform Large Area Glow Cold Plasma Tunnel at Atmospheric Pressure,” Japan. J. Appl. Phys. vol. 48, pp. 096003(1-3), 2009.

[37] K. S. Birdi, D. T. Vu, and A. Winter, “A Study of the Evaporation Rates of Small Water Drops Placed on a Solid Surface,” J. Phys. Chem., vol. 93, pp. 3702-3703, 1989.

[38] R. Defay, I. Prigogine, and A. Bellemans, "Surface tension and adsorption". (Wiley, New York, 1966) p.432.

[39] H. Zhou, Y. Yao, Q. Chen, G. Li, and S. Yao, “A facile microfluidic strategy for measuring interfacial tension,” Appl. Phys. Lett. vol. 103, pp. 234102 (1-4), 2013.

[40] P. A. Thompson and S. M. Troian, “A general boundary condition for liquid flow at solid surfaces,” Nature, vol. 389, pp. 360-362, 1997.

[41] L. Bocquet and J.-L. Barrat, “Jean-Louis Barrat, Flow boundary conditions from nano- to micro-scales,” Soft Matter, vol. 3, pp. 685-693, 2007.

[42] R. S. Voronov, D. V. Papavassiliou, and L. L. Lee, “Boundary slip and wetting properties of interfaces: Correlation of the contact angle with the slip length,” J. Chem. Phys., vol. 124, pp. 204701(1-10), 2006.

[43] M. Sakai, M. Nishimuram, Y. Morii, T. Furuta, T. Isobe, A. Fujishima, and A. Nakajima, “Reduction of fluid friction on the surface coated with TiO_2 photocatalyst under UV illumination,” J. Mater. Sci. vol. 47, pp. 8167-8173, 2012.

TABLE I. Estimated parameters and obtained data from the liquid transport experiments of the samples prepared by different plasma irradiation durations for 0, 10, 60, and 180 s.

Holes, thickness	Hole diameter [mm][a]	Plasma irradiation duration [s]	Contact angle [°][a]	Droplet radius [mm] [a,b]	Pressure difference, Pt−Pb [kPa][c]	Transport rate [nl/s]
40×40, 150μm	~14 / ~4	0	37.3 / 38.2	1.9 / 2.4	1.6	~0
	~14 / ~4	10	35.9 / 4.4	2.0 / 38	6.9	~0.8
	~14 / ~4	60	40.5 / 4.1	1.9 / 39	7.28	~1.7
	~14 / ~4	180	38.9 / 5.1	1.9 / 34	7.23	~3.9
10×10, 200μm	~13 / ~3	180	48.0 / 4.5	1.4 / 37	10	~0.1
	~18 / ~5	180	48.4 / 4.2	1.5 / 36	9.3	~2.0
	~23 / ~6	180	54.5 / 4.3	1.2 / 40	11.76	~3.8

[a] Data were separately obtained on top and bottom surfaces; (top / bottom).
[b] Droplets volume on top and bottom surfaces are ~1 μl and ~2 μl, respectively.
[c] P_t is the droplet pressure on top and P_b is the droplet pressure on bottom surfaces.

Figure captions

Figure 1: Optical microscopy images of (a) top surface and (b) bottom surface of glass substrate with holes. (c) Cross-sectional scanning electron microscopy (SEM) image of a glass substrate with high-aspect-ratio, micro-sized holes. (d) Schematic illustration of non-equilibrium atmospheric pressure plasma excited by a 7 $kV_{0\text{-}P}$ AC power supply at a frequency of 60 Hz.

Figure 2: Liquid transportation evaluation method. (a) Contact angle image of a droplet. (b) Schematic illustration of analyzing droplet volumes V from contact angle θ, radius of droplet r_d, and contact length l_c (i.e., the length of the liquid-solid interface). (c) Schematic illustration of liquid transportation method using the pressure differential between two droplets.

Figure 3: (a) Temporal volume changes of a droplet on the surface fabricated 40 × 40 holes before and after 10, 60, and 180 s of plasma irradiation. The temporal behavior was fitted by a quadratic function.

(b) Reduction rate of volume of droplets on a surface fabricated with a 40 × 40 array of holes before and after the plasma irradiation for 10, 60, and 180 s. The dotted line shows the evaporation rate of a water droplet (1 μl) on a flat glass surface.

Figure 4: Liquid transportation rates for different hole diameters after 180 s of plasma

irradiation using glass substrates fabricated with a 10 × 10 array of holes (red filled circles) and 40 × 40 holes (blue filled squares). Data were fitted by a quartic function (solid line). Dashed line draws the quartic line normalizing for the data of 40 × 40 holes (blue filled squares) with 1600 holes, 150 μm thickness, and 7 kPa pressure.

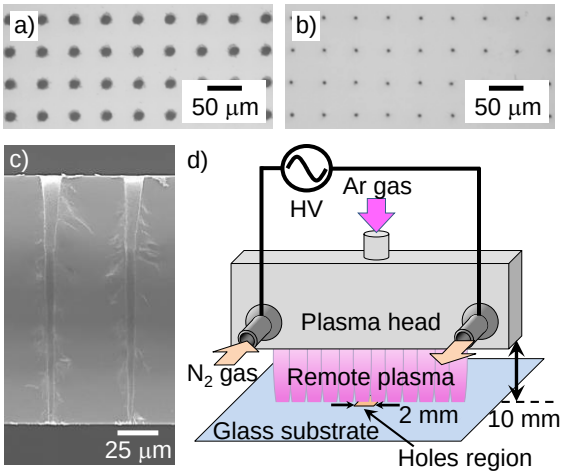
a)
50 μm
b)
50 μm
c)
25 μm
d)
HV
Ar gas
Plasma head
N2 gas
Remote plasma
2 mm
10 mm
Glass substrate
Holes region

Fig. 1

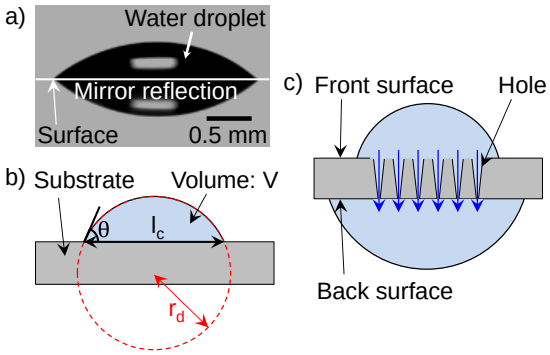
a)
Water droplet
Mirror reflection
Surface
0.5 mm
b)
Substrate
Volume: V
θ
l_c
r_d
c)
Front surface
Hole
Back surface

Fig. 2

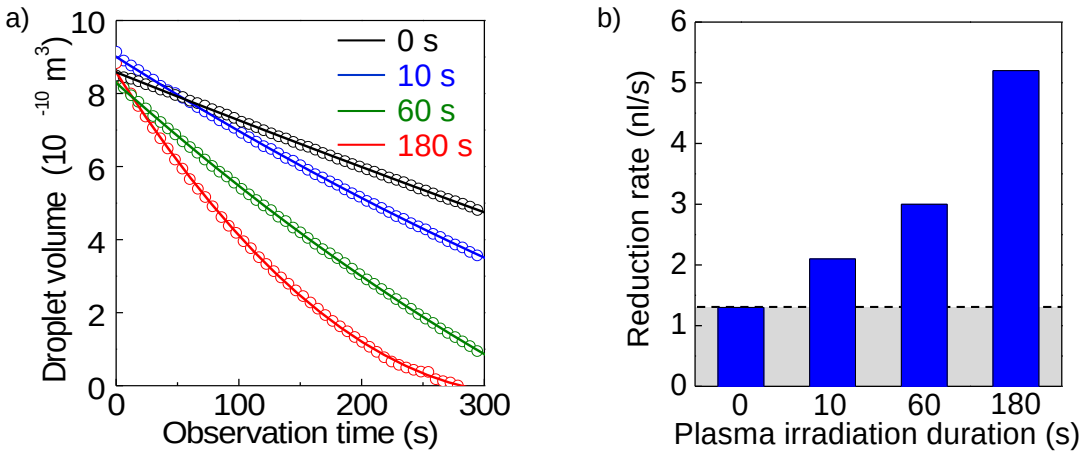
a)
Droplet volume (10 -10 m3)
Observation time (s)
0 s
10 s
60 s
180 s
b)
Reduction rate (nl/s)
Plasma irradiation duration (s)

Fig. 3

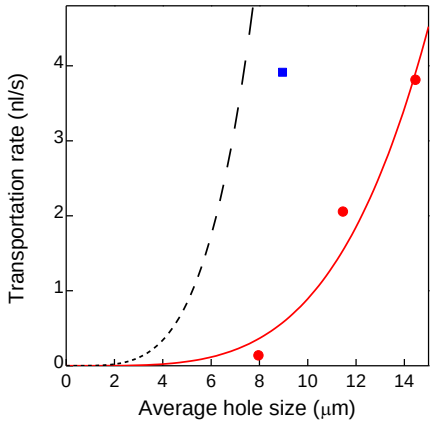
Transportation rate (nl/s)
0
1
2
3
4
0
2
4
6
8
10
12
14
Average hole size (μm)

Fig. 4